Electronic Supplementary Information for
Calcium bridging drives polysaccharide co-adsorption to a proxy sea surface microlayer

*Kimberly A. Carter-Fenk,[a] Abigail C. Dommer,[b] Michelle E. Fiamingo,[a] Jeongin J. Kim,[a] Rommie E. Amaro,[b] and Heather C. Allen[a]**

a. Department of Chemistry and Biochemistry, The Ohio State University, Columbus, OH 43210, USA
b. Department of Chemistry and Biochemistry, University of California, San Diego, La Jolla, CA 92093, USA

Corresponding Author

* Heather C. Allen (allen@chemistry.ohio-state.edu)

Figures Quick Reference

Tables Quick Reference

Table of Contents

Molecular Dynamics Systems

For the systems containing Ca^{2+}, all negative charges were balanced using random placement of calcium ions and otherwise balanced with sodium. Identical systems without alginate were also constructed as controls. The system was simulated using constant number, volume and temperature (NVT) with temperature controlled via Langevin dynamics[1] with a coupling constant of 1 ps. The equations of motion were integrated with a timestep of 2 fs, with long-range electrostatics calculated every other timestep using the Particle Mesh Ewald method with a cutoff of 12 Å.[2] A correction was applied to prevent center of mass drift due to PME by enabling the zeroMomentum parameter. The systems were energy-minimized and equilibrated for 800 ps. All simulations were performed on an AgilityValue Tower AMD ROME Workstation (Applied Data Systems Inc., Poway, CA) equipped with an NVIDIA GeForce RTX 3090 Graphics Card (Santa Clara, CA).

Given that classical non-polarizable force fields often fail to accurately represent the interactions between ions, we use a version of the additive CHARMM36 force field with an NBFIX correction (July 2018) in combination with the TIP3 water model. The NBFIX, incorporated directly into the parameters used in this work, accounts for the electronically shielded interactions between the multivalent calcium cation and the carboxylate group on the alginate. The NBFIX also accounts for the interaction between calcium and TIP3 water as well as calcium and the palmitic acid headgroups. See references for more information.[3–5]

Polarizable force fields, which are more accurate in terms of reproducing thermodynamic properties than non-polarizable force fields like CHARMM36, are much more computationally expensive. Our computational work is a simple validation of experimental results; it does not rely on precise thermodynamic calculations, and rigorous parameterization of the divalent cations is beyond the scope of this work. Furthermore, the NBFIX modification of the force field has been

shown to reasonably reproduce experimental observations of calcium binding interactions, including with peptides, LPS, saccharides, carboxylates, and phosphates.[4,6–8]

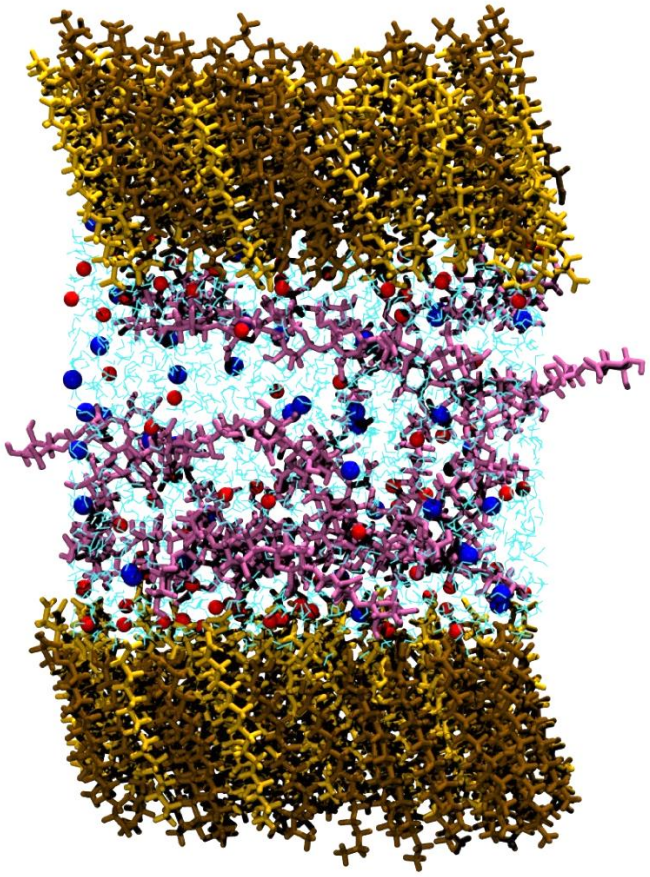

Fig. S1. Example of a molecular dynamics monolayer system set up to include alginate. Pictured: palmitic acid (brown, licorice representation), palmitate (yellow, licorice), water (cyan, lines) alginate (mauve, licorice), calcium (red, Van der Waals) and sodium (blue, Van der Waals). Above and below the monolayers is a vacuum region where no molecules were placed to approximate atmospheric air pressure.

Calculations and Data

a. Mean molecular area data

Mean molecular area (MMA) data of the d_{31}-palmitic acid and d_{33}-cetyl alcohol monolayers measured at constant surface pressure are tabulated below. Alginate consistently expands the monolayer relative to the salt water subphase, and the magnitude of monolayer expansion is greater at 5 mN/m than at 25 mN/m. Enhanced dispersion interactions between the lipid alkyl chains and increased exchange interactions likely push alginate out of the plane of the compressed monolayer.

Table S1. Average mean molecular area values (Å^2/molecule) and one standard deviation from the mean (σ, Å^2/molecule) of d_{31}-palmitic acid (d_{31}-PA) and d_{33}-cetyl alcohol (d_{33}-CA) monolayers measured at constant surface pressures 5 mN/m and 25 mN/m.

Monolayer & Subphase	5 mN/m		25 mN/m	
	MMA	σ	MMA	σ
d_{31}-PA, 0.47 M NaCl, pH 8.2	22.66	0.29	20.57	0.33
d_{31}-PA, 50 ppm Alginate, 0.47 M NaCl, pH 8.2	25.48	0.44	21.50	0.44
d_{31}-PA, 0.47 M NaCl, 10 mM $CaCl_2$, pH 8.2	22.36	0.16	20.92	0.11
d_{31}-PA, 50 ppm Alginate, 0.47 M NaCl, 10 mM $CaCl_2$, pH 8.2	23.27	0.65	21.56	0.32
d_{31}-PA, 0.47 M NaCl, 10 mM $CaCl_2$, pH 5.8	25.21	0.24	22.67	0.20
d_{31}-PA, 50 ppm Alginate, 0.47 M NaCl, 10 mM $CaCl_2$, pH 5.8	27.29	0.48	22.99	0.92
d_{33}-CA, 0.47 M NaCl, 10 mM $CaCl_2$, pH 8.2	20.62	0.15	17.85	0.09
d_{33}-CA, 50 ppm Alginate, 0.47 M NaCl, 10 mM $CaCl_2$, pH 8.2	21.91	0.08	18.72	0.05
d_{31}-PA, 0.47 M NaCl, 10 mM $MgCl_2$, pH 8.2	24.27	0.04	21.40	0.14
d_{31}-PA, 50 ppm Alginate, 0.47 M NaCl, 10 mM $MgCl_2$, pH 8.2	26.51	0.13	22.08	0.17
d_{31}-PA, 0.47 M NaCl, 53 mM $MgCl_2$, pH 8.2	24.17	0.10	21.80	0.09
d_{31}-PA, 50 ppm Alginate, 0.47 M NaCl, 53 mM $MgCl_2$, pH 8.2	27.06	0.43	22.86	0.27

Table S2. The ratio of d_{31}-palmitic acid (d_{31}-PA) and d_{33}-cetyl alcohol (d_{33}-CA) MMA values (Alg/SW) and propagated error corresponding to the 50 ppm alginate subphase MMA divided by the seawater subphase MMA.

Monolayer & Subphase	5 mN/m		25 mN/m	
	Alg/SW	Error	Alg/SW	Error
d_{31}-PA, 0.47 M NaCl, pH 8.2	1.124	0.022	1.045	0.026
d_{31}-PA, 0.47 M NaCl, 10 mM $CaCl_2$, pH 8.2	1.041	0.029	1.030	0.016
d_{31}-PA, 0.47 M NaCl, 10 mM $CaCl_2$, pH 5.8	1.083	0.020	1.014	0.041
d_{33}-CA, 0.47 M NaCl, 10 mM $CaCl_2$, pH 8.2	1.062	0.008	1.049	0.005
d_{31}-PA, 0.47 M NaCl, 10 mM $MgCl_2$, pH 8.2	1.092	0.005	1.032	0.010
d_{31}-PA, 0.47 M NaCl, 53 mM $MgCl_2$, pH 8.2	1.120	0.017	1.048	0.012

b. D-guluronate and d_{31}-palmitic acid vibrational frequency calculations

To distinguish between peaks corresponding to the d_{31}-palmitic acid monolayer or the co-adsorbed alginate, harmonic vibrational frequency calculations were performed using Q-Chem v. 5.3.1.[9] D-guluronic acid, an alginate monomer primarily responsible for cation binding, was selected to model the alginate vibrational modes (Figure S1a).[10–12] Both protonated d_{31}-palmitic acid (Figure S1b) and deprotonated d_{31}-palmitate (Figure S1c) were modeled, and the atomic mass of 2.01410 was used for the deuterium atoms.[13] Geometry optimization and harmonic frequency analysis were performed at the EDF2/6-31+G* level of theory.[14] Frequencies, intensities, and vibrational mode assignments within the frequency region of the carboxylic acid headgroup and the C-D bending modes (1090-1850 cm^{-1}) are tabulated in Tables S3-S5.

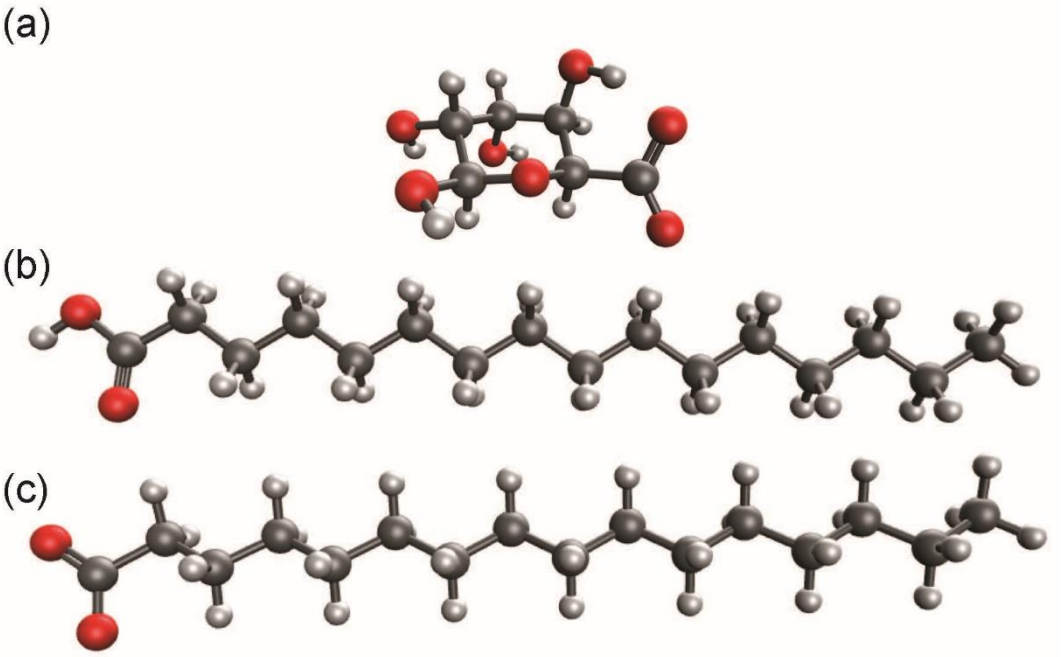

Fig. S2. Geometry optimized structures of (a) D-guluronate, (b) d_{31}-palmitic acid, and (c) d_{31}-palmitate.

Table S3. Harmonic vibrational frequencies, intensities, and vibrational mode assignments of D-guluronate.

Wavenumber (cm^{-1})	Intensity (km/mol)	Mode Assignments
1094.24	111.741	C-O-H Bending, C-O-C Stretching
1100.50	145.998	C-OH Stretching
1116.31	80.623	C-O-C Stretching, C-O-H Bending
1148.48	211.874	C-O-H Stretching, C-H Wagging
1154.90	2.637	C-O-H Stretching and Bending
1206.32	34.863	C-O-H Bending, C-H Wagging
1242.62	32.793	C-H Wagging, C-O-H Bending
1264.93	32.675	C-H Wagging, C-O-H Bending
1297.55	18.810	C-H Wagging, C-O-H Bending
1317.06	32.035	C-H Wagging, C-O-H Bending
1325.07	15.798	C-H Wagging, C-O-H Bending
1340.30	18.708	C-H Wagging, C-O-H Bending
1352.16	121.662	C-H Wagging, C-O-H Bending, COO^- Symmetric Stretching
1356.34	27.790	C-H Wagging, C-O-H Bending, COO^- Symmetric Stretching
1391.73	127.213	COO^- Symmetric Stretching, C-H Wagging
1400.35	16.914	C-H Wagging, C-O-H Bending
1411.78	25.561	C-O-H Bending, C-H Wagging
1439.87	44.051	C-O-H Bending, C-H Wagging
1474.40	2.861	C-O-H Bending, C-H Wagging
1547.29	384.253	C-O-H Bending, COO^- Asymmetric Stretching
1725.18	423.674	COO^- Asymmetric Stretching, C-O-H Bending

Table S4. Harmonic vibrational frequencies, intensities, and vibrational mode assignments of d_{31}-palmitic acid.

Wavenumber (cm^{-1})	Intensity (km/mol)	Mode Assignments
1092.09	0.403	CD_3 Bending, CD_2 Bending & Wagging
1093.01	4.856	CD_3 Bending
1093.67	7.022	CD_2 Bending
1108.35	13.932	CD_2 Bending & Wagging, CD_3 Bending
1116.04	2.674	CD_2 Bending & Wagging
1117.22	0.663	CD_2 Bending & Wagging
1119.12	0.914	CD_2 Bending & Wagging
1121.34	0.634	CD_2 Bending
1123.82	1.570	CD_2 Bending
1125.90	0.640	CD_2 Bending
1127.50	11.375	CD_2 Bending
1128.73	8.575	CD_2 Bending, CD_3 Bending
1132.35	1.303	CD_2 Bending & Wagging, CD_3 Bending
1141.51	14.964	CD_2 Bending, C-O-H Bending & Stretching
1150.56	15.657	CD_2 Bending & Wagging, C-O-H Bending & Stretching
1159.16	46.521	C-O-H Bending & Stretching, CD_2 Bending & Wagging
1167.89	4.210	CD_2 Bending & Wagging, C-O-H Bending & Stretching
1177.22	4.233	CD_2 Bending, C-O-H Bending & Stretching
1189.07	65.964	C-O-H Bending & Stretching, CD_2 Wagging
1216.54	59.856	C-O-H Bending & Stretching, CD_2 Wagging
1241.05	15.368	CD_2 Wagging, C-O-H Bending
1260.91	6.855	CD_2 Wagging, C-O-H Bending
1274.81	0.569	CD_2 Wagging, C-O-H Bending
1282.93	0.528	CD_2 Wagging, C-O-H Bending
1286.54	0.032	CD_2 Wagging, C-O-H Bending
1288.46	0.160	CD_2 Wagging, C-O-H Bending
1369.64	120.711	C-O-H Bending & Stretching
1827.90	299.335	C=O Stretching, C-O-H Bending

Table S5. Harmonic vibrational frequencies, intensities, and vibrational mode assignments of d_{31}-palmitate.

Wavenumber (cm^{-1})	Intensity (km/mol)	Mode Assignments
1091.89	7.209	CD_3 Bending, CD_2 Bending & Wagging
1092.92	4.719	CD_3 Bending
1093.94	5.964	CD_2 Bending & Wagging, CD_3 Bending
1108.52	0.333	CD_2 Bending & Wagging, CD_3 Bending
1114.79	0.338	CD_2 Bending & Wagging
1116.53	0.014	CD_2 Bending & Wagging
1118.41	0.561	CD_2 Bending & Wagging, CD_3 Bending
1120.73	0.006	CD_2 Bending & Wagging, CD_3 Bending
1123.15	1.640	CD_2 Bending, CD_3 Bending
1125.37	0.002	CD_2 Bending, CD_3 Bending
1127.13	10.458	CD_2 Bending
1127.55	0.296	CD_2 Bending, CD_3 Bending
1131.37	0.628	CD_2 Bending & Wagging, CD_3 Bending
1140.96	0.701	CD_2 Bending & Wagging, CD_3 Bending
1149.66	0.109	CD_2 Bending & Wagging
1162.08	2.876	CD_2 Bending & Wagging, CD_3 Bending
1167.45	0.477	CD_2 Bending & Wagging, CD_3 Bending
1177.28	0.702	CD_2 Bending, CD_3 Bending
1198.48	0.953	CD_2 Bending & Wagging, CD_3 Bending
1228.77	0.582	CD_2 Bending & Wagging, CD_3 Bending
1250.96	1.753	CD_2 Wagging, CD_3 Bending
1265.36	0.348	CD_2 Wagging, CD_3 Bending
1275.19	0.701	CD_2 Wagging, CD_3 Bending
1281.76	0.054	CD_2 Wagging
1285.41	0.085	CD_2 Wagging
1371.58	328.038	COO^- Symmetric Stretching
1678.00	637.505	COO^- Asymmetric Stretching

c. Carboxylate region spectral fitting

Peaks within the COOH stretching region (1150-1850 cm^{-1}) were fitted to Gaussian functions using OriginPro 9.0. The software uses the Levenberg-Marquardt algorithm to perform the nonlinear curve fitting routine. Eight points were placed along the baseline, and a 4^{th}-order polynomial function was fitted to those points and used to define the spectral baseline. Peak fitting parameters were not fixed.

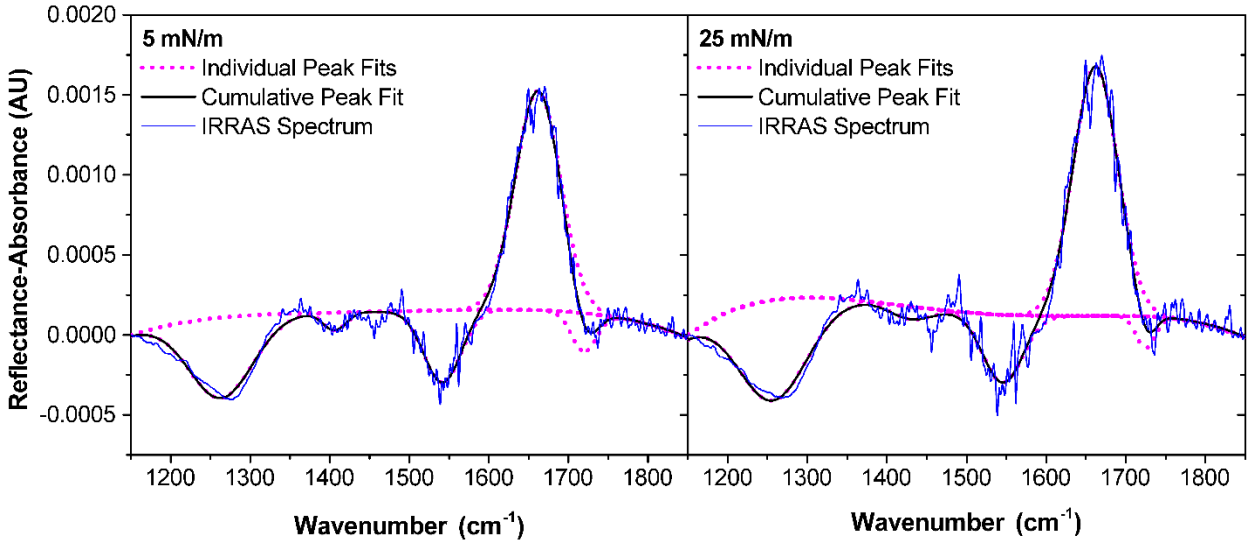

Fig. S3. IRRAS spectra and corresponding peak fits of a d_{31}-palmitic acid monolayer at 5 mN/m (left) and 25 mN/m (right) spread onto an aqueous subphase of 0.47 M NaCl at pH 8.2.

Table S6. Center wavelengths (λ, cm^{-1}), reflectance-absorbance intensities (RA Int.), peak areas, and full width at half maximum (FWHM, cm^{-1}) values of Gaussian fits to IRRAS spectra in the COOH vibrational mode region of a d_{31}-palmitic acid monolayer (5 mN/m and 25 mN/m) spread onto an aqueous subphase of 0.47 M NaCl at pH 8.2.

Vibrational Mode	5 mN/m				25 mN/m			
	Center λ	RA Int.	Area	FWHM	Center λ	RA Int.	Area	FWHM
ν C-OH	1263.5	-5.02E-04	0.0501	93.7	1256.7	-6.31E-04	0.06895	102.7
ν_S COO^-	1406.3	-1.10E-04	0.00399	34.0	1429.7	-7.92E-05	0.00509	60.4
ν_{AS} COO^-	1541.6	-4.49E-04	0.0261	54.5	1545.6	-4.23E-04	0.0263	58.4
δ H-O-H	1661.5	0.00137	0.0975	66.9	1662.0	0.00156	0.109	66.0
ν C=O	1719.6	-2.40E-04	0.00942	36.8	1725.1	-1.96E-04	0.00586	28.1

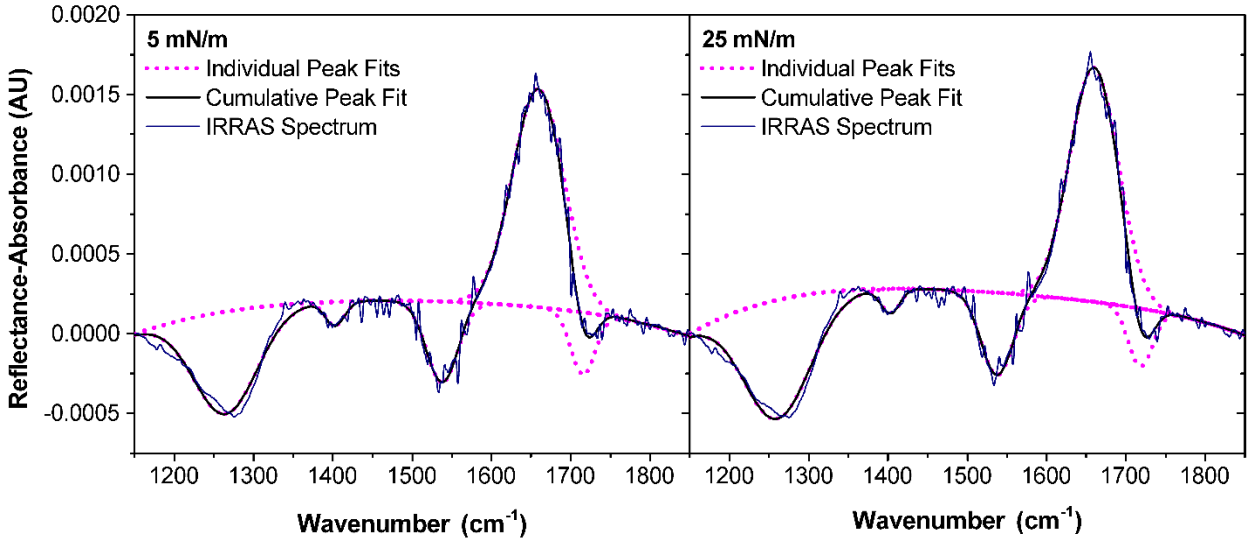

Fig. S4. IRRAS spectra and corresponding peak fits of a d_{31}-palmitic acid monolayer at 5 mN/m (left) and 25 mN/m (right) spread onto an aqueous subphase of 0.47 M NaCl and 50 ppm alginate at pH 8.2.

Table S7. Center wavelengths (λ, cm^{-1}), reflectance-absorbance intensities (RA Int.), peak areas, and full width at half maximum (FWHM, cm^{-1}) values of Gaussian fits to IRRAS spectra in the COOH vibrational mode region of a d_{31}-palmitic acid monolayer (5 mN/m and 25 mN/m) spread onto an aqueous subphase of 0.47 M NaCl and 50 ppm alginate at pH 8.2.

Vibrational Mode	5 mN/m				25 mN/m			
	Center λ	RA Int.	Area	FWHM	Center λ	RA Int.	Area	FWHM
ν C-OH	1264.7	-6.42E-04	0.0643	94.1	1260.5	-7.46E-04	0.0789	99.3
ν_S COO^-	1402.6	-1.50E-04	0.00458	28.7	1402.9	-1.53E-04	0.00461	28.3
ν_{AS} COO^-	1537.8	-5.07E-04	0.0253	46.9	1537.3	-5.16E-04	0.0260	47.3
δ H-O-H	1658.9	0.00137	0.111	76.2	1659.6	0.00147	0.114	72.6
ν C=O	1715.4	-3.88E-04	0.0149	35.9	1718.3	-3.62E-04	0.0139	36.0

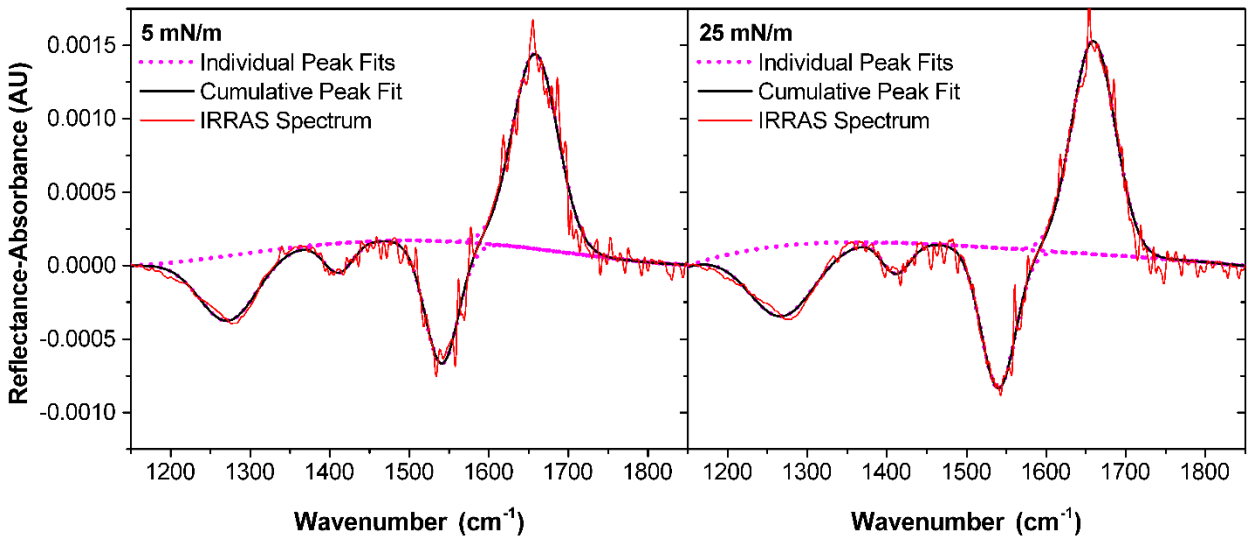

Fig. S5. IRRAS spectra and corresponding peak fits of a d_{31}-palmitic acid monolayer at 5 mN/m (left) and 25 mN/m (right) spread onto an aqueous subphase of 0.47 M NaCl and 10 mM $CaCl_2$ at pH 8.2.

Table S8. Center wavelengths (λ, cm^{-1}), reflectance-absorbance intensities (RA Int.), peak areas, and full width at half maximum (FWHM, cm^{-1}) values of Gaussian fits to IRRAS spectra in the COOH vibrational mode region of a d_{31}-palmitic acid monolayer (5 mN/m and 25 mN/m) spread onto an aqueous subphase of 0.47 M NaCl and 10 mM $CaCl_2$ at pH 8.2.

Vibrational Mode	5 mN/m				25 mN/m			
	Center λ	RA Int.	Area	FWHM	Center λ	RA Int.	Area	FWHM
ν C-OH	1272.6	-4.42E-04	0.0401	85.0	1268.2	-4.81E-04	0.0497	97.1
ν_S COO^-	1410.8	-2.03E-04	0.00908	41.9	1411.5	-2.12E-04	0.00933	41.3
ν_{AS} COO^-	1540.6	-8.35E-04	0.0439	49.4	1539.9	-9.57E-04	0.0515	50.6
δ H-O-H	1658.0	0.00133	0.0946	67.0	1659.5	0.00145	0.0994	64.4

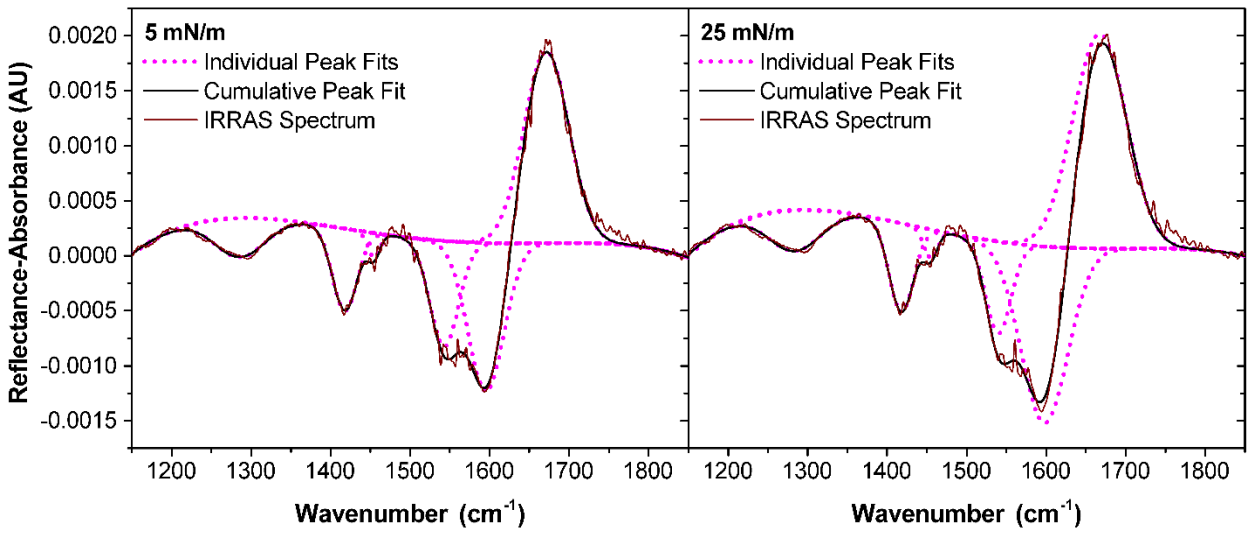

Fig. S6. IRRAS spectra and corresponding peak fits of a d_{31}-palmitic acid monolayer at 5 mN/m (left) and 25 mN/m (right) spread onto an aqueous subphase of 0.47 M NaCl, 10 mM $CaCl_2$, and 50 ppm alginate at pH 8.2.

Table S9. Center wavelengths (λ, cm^{-1}), reflectance-absorbance intensities (RA Int.), peak areas, and full width at half maximum (FWHM, cm^{-1}) values of Gaussian fits to IRRAS spectra in the COOH vibrational mode region of a d_{31}-palmitic acid monolayer (5 mN/m and 25 mN/m) spread onto an aqueous subphase of 0.47 M NaCl, 10 mM $CaCl_2$, and 50 ppm alginate at pH 8.2.

Vibrational Mode	5 mN/m				25 mN/m			
	Center λ	RA Int.	Area	FWHM	Center λ	RA Int.	Area	FWHM
ν C-OH	1285.7	-3.58E-04	0.0291	76.3	1283.5	-3.77E-04	0.0318	79.2
ν_S COO^- (d_{31}-Palmitate)	1417.8	-7.45E-04	0.0293	36.9	1417.8	-8.07E-04	0.0314	36.5
ν_S COO^- (Alginate)	1454.3	-2.16E-4	0.00415	18.0	1454.7	-2.54E-4	0.00558	20.7
ν_{AS} COO^- (d_{31}-Palmitate)	1543.0	9.58E-04	0.0432	42.3	1539.8	-8.34E-04	0.0336	37.9
ν_{AS} COO^- (Alginate)	1595.4	0.00135	0.0768	53.6	1597.9	-0.00160	0.118	69.0
δ H-O-H	1671.3	0.00174	0.124	66.6	1667.3	0.00195	0.164	79.0

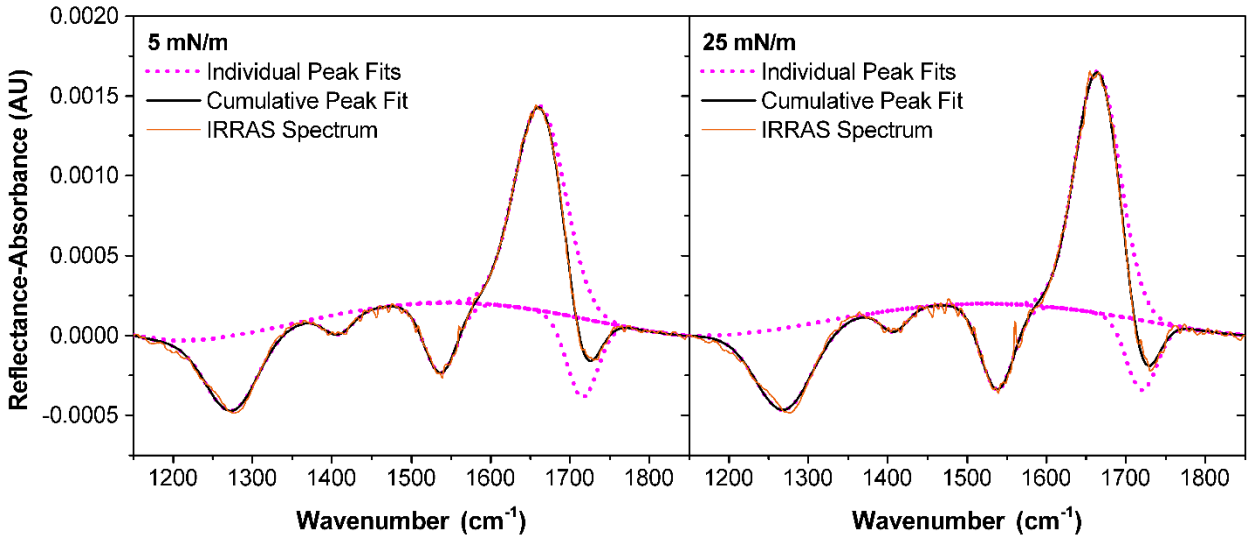

Fig. S7. IRRAS spectra and corresponding peak fits of a d_{31}-palmitic acid monolayer at 5 mN/m (left) and 25 mN/m (right) spread onto an aqueous subphase of 0.47 M NaCl and 10 mM $CaCl_2$ at pH 5.8.

Table S10. Center wavelengths (λ, cm^{-1}), reflectance-absorbance intensities (RA Int.), peak areas, and full width at half maximum (FWHM, cm^{-1}) values of Gaussian fits to IRRAS spectra in the COOH vibrational mode region of a d_{31}-palmitic acid monolayer (5 mN/m and 25 mN/m) spread onto an aqueous subphase of 0.47 M NaCl and 10 mM $CaCl_2$ at pH 5.8.

Vibrational Mode	5 mN/m				25 mN/m			
	Center λ	RA Int.	Area	FWHM	Center λ	RA Int.	Area	FWHM
ν C-OH	1274.0	-4.67E-04	0.0377	75.8	1269.6	-5.11E-04	0.0448	82.4
ν_S COO^-	1408.2	-1.27E-04	0.00570	42.0	1407.9	-1.36E-04	0.00563	38.9
ν_{AS} COO^-	1536.9	-4.40E-04	0.0225	48.0	1538.0	-5.36E-04	0.0281	49.2
δ H-O-H	1661.6	0.00128	0.102	74.9	1664.1	0.00151	0.107	66.8
ν C=O	1715.2	-4.91E-04	0.0239	45.8	1719.7	-4.36E-04	0.0209	45.0

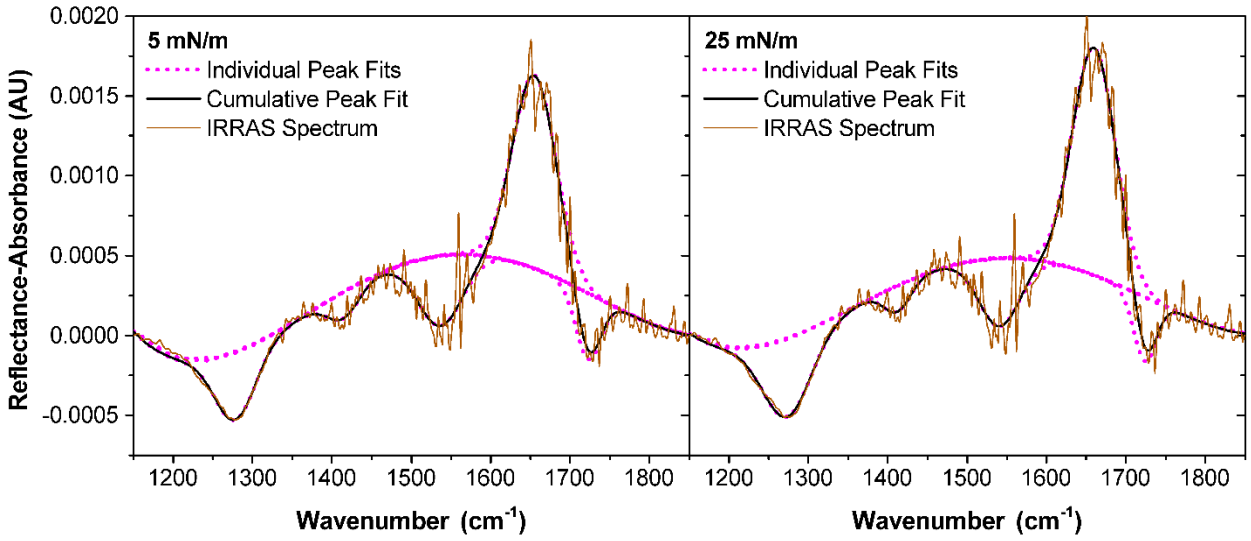

Fig. S8. IRRAS spectra and corresponding peak fits of a d_{31}-palmitic acid monolayer at 5 mN/m (left) and 25 mN/m (right) spread onto an aqueous subphase of 0.47 M NaCl, 10 mM $CaCl_2$, and 50 ppm alginate at pH 5.8.

Table S11. Center wavelengths (λ, cm^{-1}), reflectance-absorbance intensities (RA Int.), peak areas, and full width at half maximum (FWHM, cm^{-1}) values of Gaussian fits to IRRAS spectra in the COOH vibrational mode region of a d_{31}-palmitic acid monolayer (5 mN/m and 25 mN/m) spread onto an aqueous subphase of 0.47 M NaCl, 10 mM $CaCl_2$, and 50 ppm alginate at pH 5.8.

Vibrational Mode	5 mN/m				25 mN/m			
	Center λ	RA Int.	Area	FWHM	Center λ	RA Int.	Area	FWHM
ν C-OH	1278.6	-4.18E-04	0.0264	59.2	1273.6	-4.86E-04	0.0363	70.1
ν_S COO^-	1414.3	-1.67E-04	0.00834	46.8	1412.1	-1.65E-04	0.00689	39.2
ν_{AS} COO^-	1536.8	-4.42E-04	0.0314	66.8	1540.6	-4.29E-04	0.0280	61.3
δ H-O-H	1654.9	0.00121	0.0829	64.6	1659.8	0.00142	0.0969	64.0
ν C=O	1722.6	-4.12E-04	0.0162	37.0	1724.1	-4.00E-04	0.0142	33.4

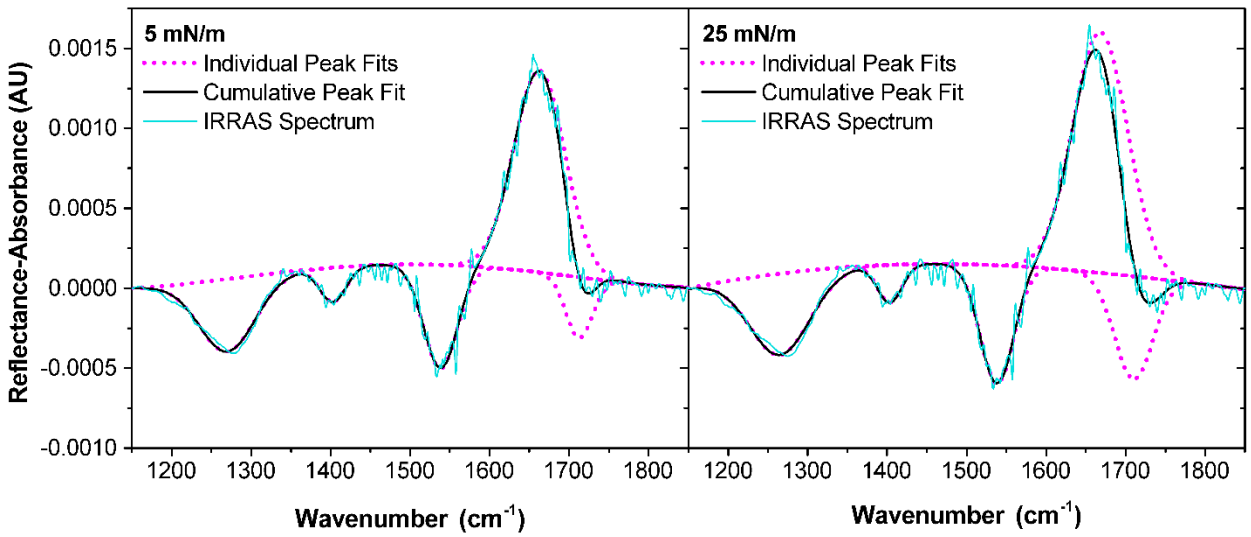

Fig. S9. IRRAS spectra and corresponding peak fits of a d_{31}-palmitic acid monolayer at 5 mN/m (left) and 25 mN/m (right) spread onto an aqueous subphase of 0.47 M NaCl and 10 mM $MgCl_2$ at pH 8.2.

Table S12. Center wavelengths (λ, cm^{-1}), reflectance-absorbance intensities (RA Int.), peak areas, and full width at half maximum (FWHM, cm^{-1}) values of Gaussian fits to IRRAS spectra in the COOH vibrational mode region of a d_{31}-palmitic acid monolayer (5 mN/m and 25 mN/m) spread onto an aqueous subphase of 0.47 M NaCl and 10 mM $MgCl_2$ at pH 8.2.

Vibrational Mode	5 mN/m				25 mN/m			
	Center λ	RA Int.	Area	FWHM	Center λ	RA Int.	Area	FWHM
ν C-OH	1270.3	-4.53E-04	0.0398	82.6	1265.3	-5.08E-04	0.0484	89.4
ν_S COO^-	1403.0	-2.15E-04	0.00888	38.8	1403.3	-2.36E-04	0.00911	36.3
ν_{AS} COO^-	1538.4	-6.46E-04	0.0347	50.5	1538.2	-7.39E-04	0.0393	49.9
δ H-O-H	1662.6	0.00126	0.102	75.9	1668.1	0.00151	0.130	80.9
ν C=O	1712.6	-3.79E-04	0.0159	39.5	1710.1	-6.41E-04	0.0388	56.8

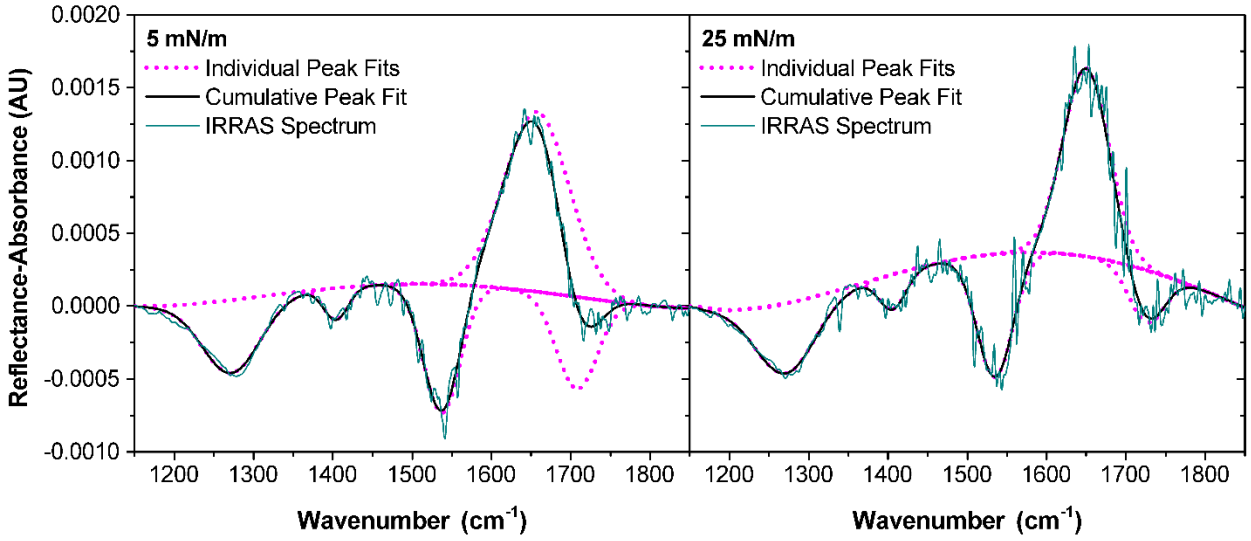

Fig. S10. IRRAS spectra and corresponding peak fits of a d_{31}-palmitic acid monolayer at 5 mN/m (left) and 25 mN/m (right) spread onto an aqueous subphase of 0.47 M NaCl, 10 mM $MgCl_2$, and 50 ppm alginate at pH 8.2.

Table S13. Center wavelengths (λ, cm^{-1}), reflectance-absorbance intensities (RA Int.), peak areas, and full width at half maximum (FWHM, cm^{-1}) values of Gaussian fits to IRRAS spectra in the COOH vibrational mode region of a d_{31}-palmitic acid monolayer (5 mN/m and 25 mN/m) spread onto an aqueous subphase of 0.47 M NaCl, 10 mM $MgCl_2$, and 50 ppm alginate at pH 8.2.

Vibrational Mode	5 mN/m				25 mN/m			
	Center λ	RA Int.	Area	FWHM	Center λ	RA Int.	Area	FWHM
ν C-OH	1272.1	-4.99E-04	0.0455	85.5	1271.4	-4.78E-04	0.0439	86.2
ν_S COO^-	1404.0	-2.19E-04	0.00840	36.1	1405.7	-2.40E-04	0.0101	39.6
ν_{AS} COO^-	1537.3	-8.85E-04	0.0512	54.4	1534.9	-8.45E-04	0.0478	53.2
δ H-O-H	1657.2	0.00123	0.126	96.2	1649.7	0.00129	0.0944	68.7
ν C=O	1707.7	-6.31E-04	0.0405	60.3	1726.2	-3.58E-04	0.0200	52.4

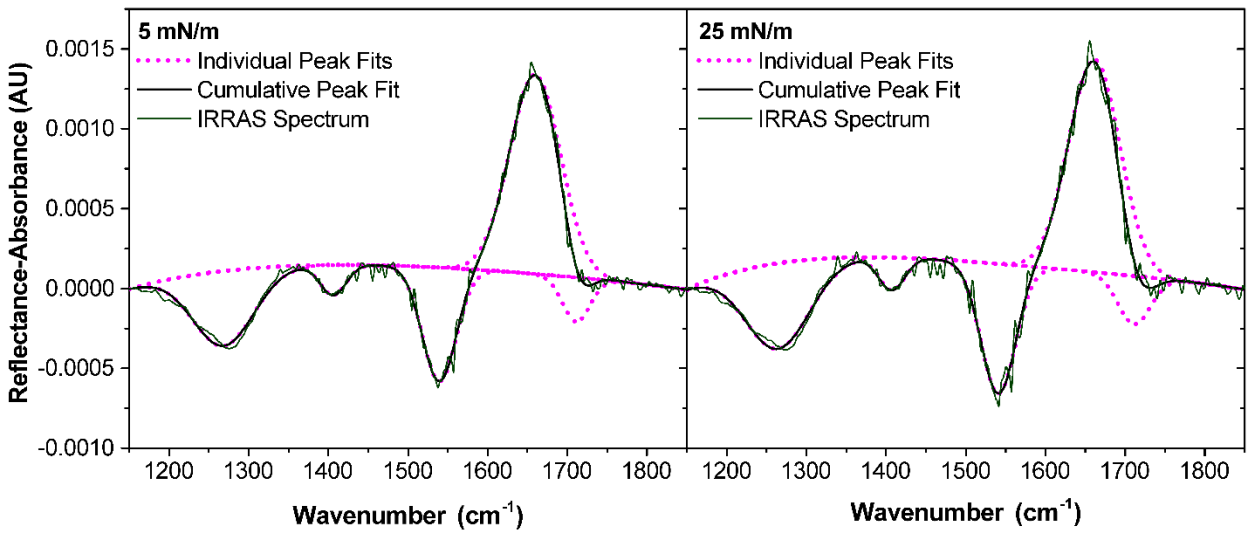

Fig. S11. IRRAS spectra and corresponding peak fits of a d_{31}-palmitic acid monolayer at 5 mN/m (left) and 25 mN/m (right) spread onto an aqueous subphase of 0.47 M NaCl and 53 mM $MgCl_2$ at pH 8.2.

Table S14. Center wavelengths (λ, cm^{-1}), reflectance-absorbance intensities (RA Int.), peak areas, and full width at half maximum (FWHM, cm^{-1}) values of Gaussian fits to IRRAS spectra in the COOH vibrational mode region of a d_{31}-palmitic acid monolayer (5 mN/m and 25 mN/m) spread onto an aqueous subphase of 0.47 M NaCl and 53 mM $MgCl_2$ at pH 8.2.

Vibrational Mode	5 mN/m				25 mN/m			
	Center λ	RA Int.	Area	FWHM	Center λ	RA Int.	Area	FWHM
ν C-OH	1268.6	-4.69E-04	0.0447	89.6	1264.1	-5.37E-04	0.0543	95.1
ν_S COO^-	1406.0	-1.89E-04	0.00768	38.1	1406.8	-2.05E-04	0.00834	38.3
ν_{AS} COO^-	1539.3	-7.13E-04	0.0381	50.1	1540.6	-8.13E-04	0.0445	51.4
δ H-O-H	1659.5	0.00125	0.100	75.6	1661.1	0.00133	0.107	75.4
ν C=O	1711.0	-2.77E-04	0.0119	40.4	1711.1	-3.01E-04	0.0154	48.2

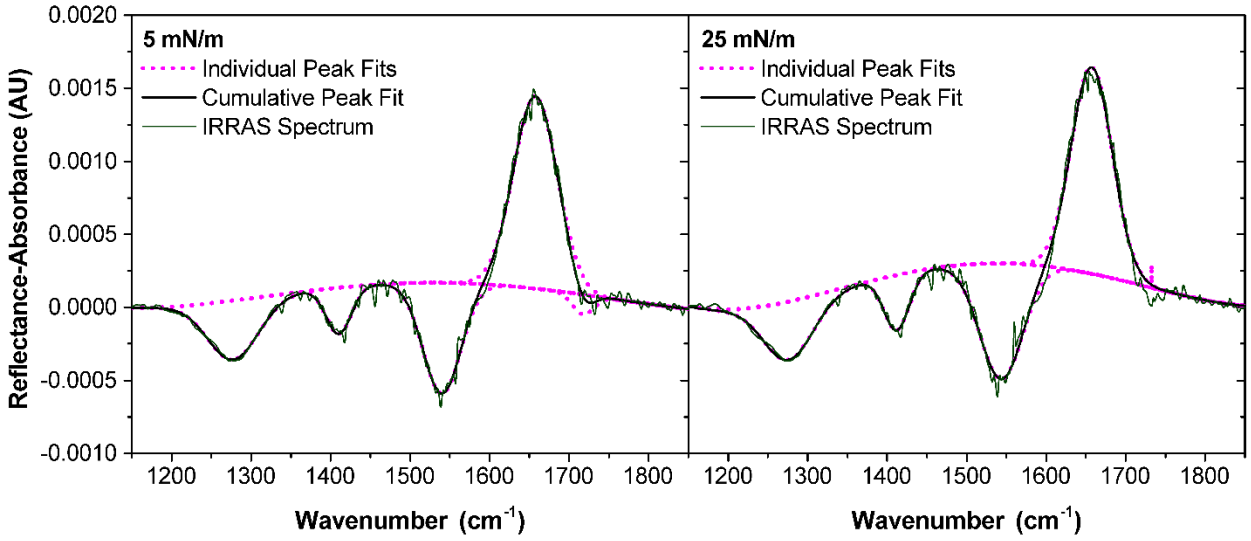

Fig. S12. IRRAS spectra and corresponding peak fits of a d_{31}-palmitic acid monolayer at 5 mN/m (left) and 25 mN/m (right) spread onto an aqueous subphase of 0.47 M NaCl, 53 mM $MgCl_2$, and 50 ppm alginate at pH 8.2.

Table S15. Center wavelengths (λ, cm^{-1}), reflectance-absorbance intensities (RA Int.), peak areas, and full width at half maximum (FWHM, cm^{-1}) values of Gaussian fits to IRRAS spectra in the COOH vibrational mode region of a d_{31}-palmitic acid monolayer (5 mN/m and 25 mN/m) spread onto an aqueous subphase of 0.47 M NaCl, 53 mM $MgCl_2$, and 50 ppm alginate at pH 8.2.

Vibrational Mode	5 mN/m				25 mN/m			
	Center λ	RA Int.	Area	FWHM	Center λ	RA Int.	Area	FWHM
ν C-OH	1277.5	-4.05E-04	0.0322	74.7	1276.1	-3.97E-04	0.0308	72.9
ν_S COO^-	1410.3	-3.18E-04	0.0126	37.1	1412.1	-3.80E-04	0.0150	37.2
ν_{AS} COO^-	1539.9	-7.59E-04	0.0453	56.0	1543.5	-7.94E-04	0.0540	63.8
δ H-O-H	1657.6	0.00132	0.0910	64.9	1657.4	0.00141	0.0916	60.9
ν C=O	1717.7	-1.35E-04	0.00451	31.3	1732.6	1.60E-04	7.92E-07	0.00464

d. d_{33}-Cetyl alcohol IRRAS spectral analysis

The carboxylic acid stretching region (1150-1850 cm^{-1}) was analyzed for the d_{33}-cetyl alcohol spectra to further examine the extent of alginate co-adsorption to the monolayer (Fig. S13). Cetyl alcohol only exhibits the C-OH stretching mode, so any carboxylic acid peaks can be attributed to alginate co-adsorption. Neither the ν_S COO^-, ν_{AS} COO^-, nor the ν C=O stretches appear at either surface pressure, indicating no alginate co-adsorption. The δ H-O-H mode red shifts in response

to alginate within the aqueous subphase, possibly caused by alginate solvation within the probing region of IRRAS.

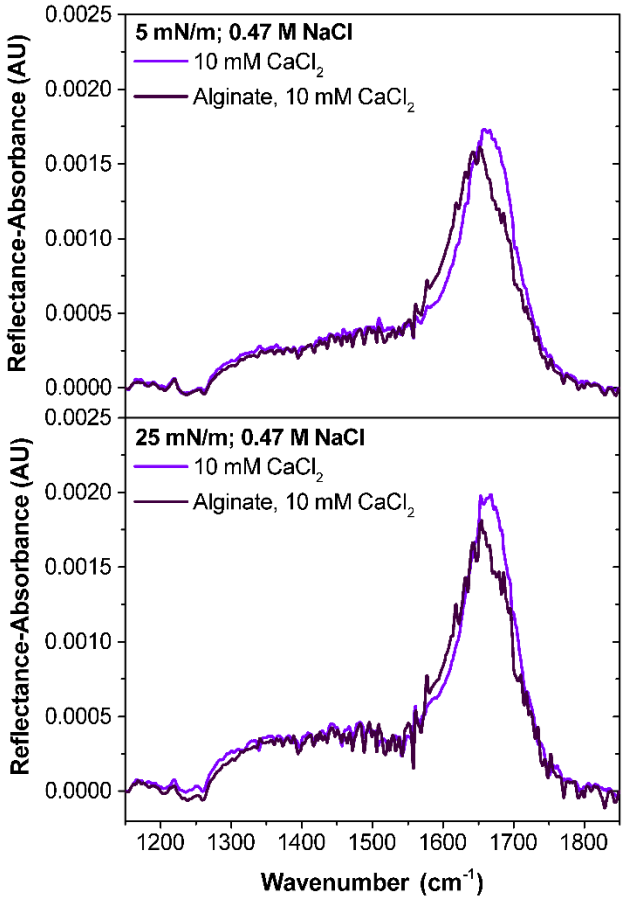

Fig. S13. IRRAS spectra of d_{33}-cetyl alcohol collected and analyzed within the COOH stretching region at constant surface pressures of 5 mN/m (top) and 25 mN/m (bottom). The light purple curves correspond to the monolayer spread onto a 0.47 M NaCl and 10 mM $CaCl_2$ subphase at pH 8.2. The dark purple curves correspond to the monolayer spread onto a 0.47 M NaCl, 10 mM $CaCl_2$, and 50 ppm alginate subphase. All spectra represent averages of at least triplicate measurements.

e. CD_2 scissoring mode analysis

The CD_2 scissoring mode region (1070-1110 cm^{-1}) was analyzed using OriginPro 9.0. A baseline was fitted to a line between the two endpoints of the region, and then the baseline was

subtracted from the spectrum. Following baseline subtraction, the center frequency of the CD_2 scissoring mode was determined with the Peak Analyzer tool in Origin.

Table S16. Center wavelengths (λ, cm^{-1}) of the IRRAS CD_2 scissoring mode of d_{31}-palmitic acid (d_{31}-PA) and d_{33}-cetyl alcohol (d_{33}-CA) monolayers measured at constant surface pressures 5 mN/m and 25 mN/m.

Monolayer & Subphase	**CD_2 Scissoring Mode λ**	
	5 mN/m	**25 mN/m**
d_{31}-PA, 0.47 M NaCl, pH 8.2	1089.5	1089.0
d_{31}-PA, 50 ppm Alginate, 0.47 M NaCl, pH 8.2	1089.5	1089.0
d_{31}-PA, 0.47 M NaCl, 10 mM $CaCl_2$, pH 8.2	1089.4	1089.4
d_{31}-PA, 50 ppm Alginate, 0.47 M NaCl, 10 mM $CaCl_2$, pH 8.2	1089.4	1089.5
d_{31}-PA, 0.47 M NaCl, 10 mM $CaCl_2$, pH 5.8	1089.5	1089.5
d_{31}-PA, 50 ppm Alginate, 0.47 M NaCl, 10 mM $CaCl_2$, pH 5.8	1089.5	1089.5
d_{33}-CA, 0.47 M NaCl, 10 mM $CaCl_2$, pH 8.2	1089.0	1089.0
d_{33}-CA, 50 ppm Alginate, 0.47 M NaCl, 10 mM $CaCl_2$, pH 8.2	1089.0	1089.0
d_{31}-PA, 0.47 M NaCl, 10 mM $MgCl_2$, pH 8.2	1089.5	1089.0
d_{31}-PA, 50 ppm Alginate, 0.47 M NaCl, 10 mM $MgCl_2$, pH 8.2	1089.5	1089.0
d_{31}-PA, 0.47 M NaCl, 53 mM $MgCl_2$, pH 8.2	1089.5	1089.0
d_{31}-PA, 50 ppm Alginate, 0.47 M NaCl, 53 mM $MgCl_2$, pH 8.2	1089.5	1089.5

f. Radial distribution and number density profiles

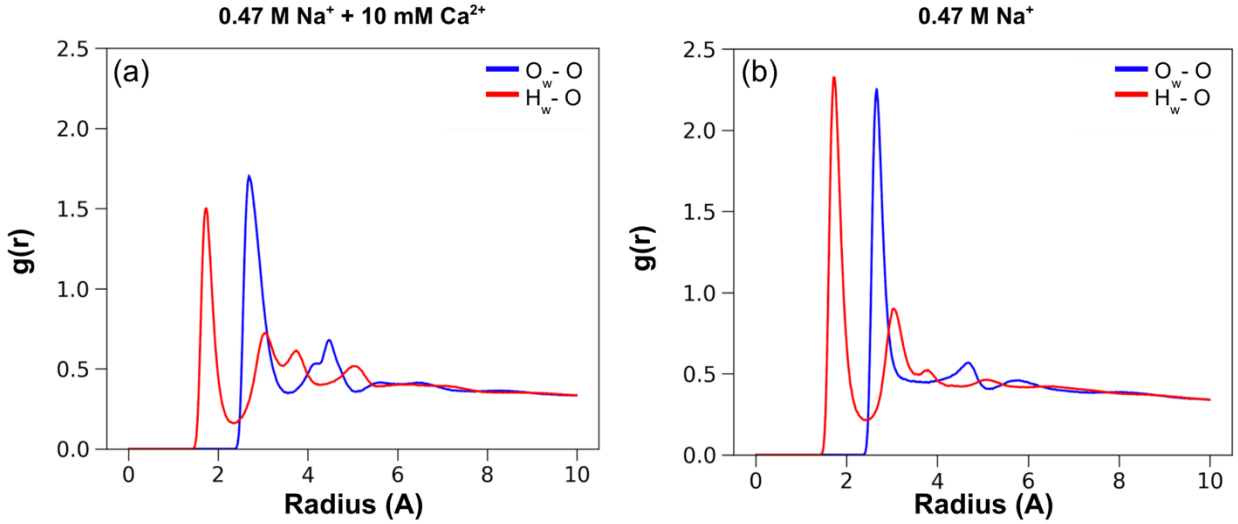

Fig. S14. RDF of water O_w and H_w with respect to palmitate headgroup -OH oxygen in the presence (a) and absence (b) of calcium. Both systems contain alginate in the aqueous phase.

g. d_{31}-Palmitic acid C-D stretching modes

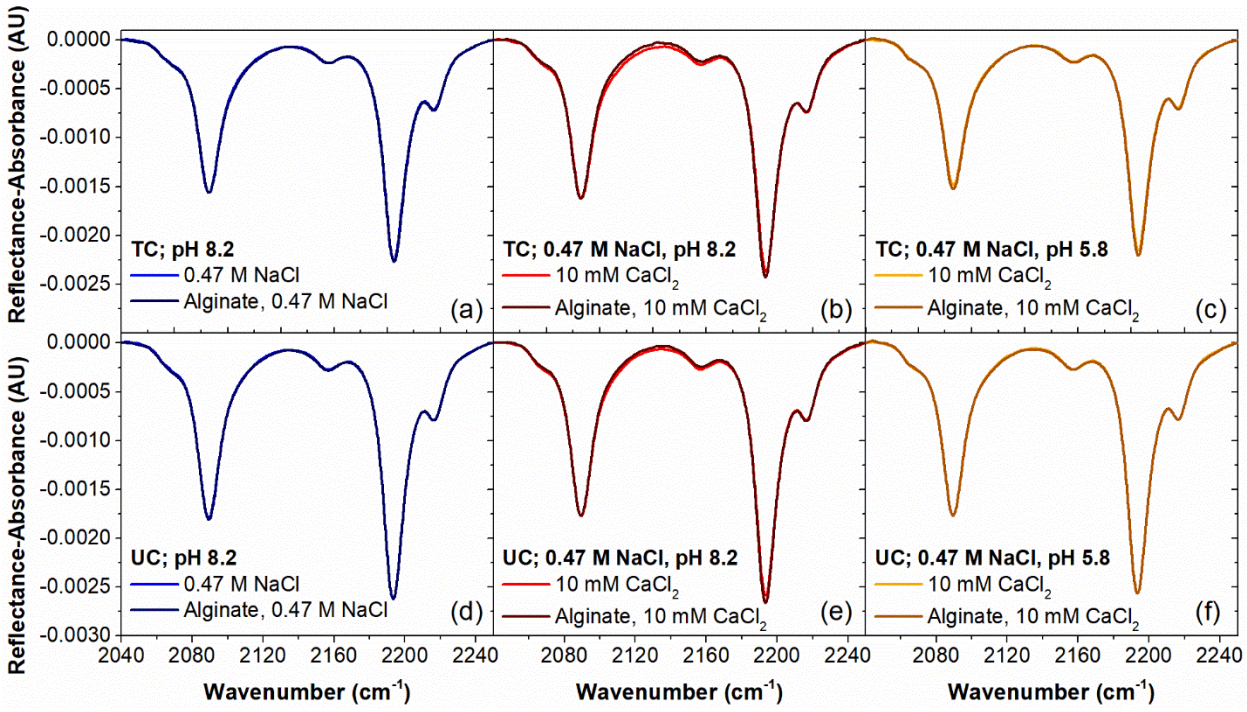

Fig. S15. IRRAS spectra of the C-D stretching mode region demonstrate no changes in the d_{31}-palmitic acid lipid tail packing with alginate co-adsorption, indicating no alginate intercalation into the monolayer. Spectral lines are color-coded to indicate differences in solution composition.

Surface pressure was held constant in the (a), (b), (c) tilted condensed (5 mN/m) and (d), (e), (f) untilted condensed (25 mN/m) phases throughout spectral acquisition.

h. Local order parameters

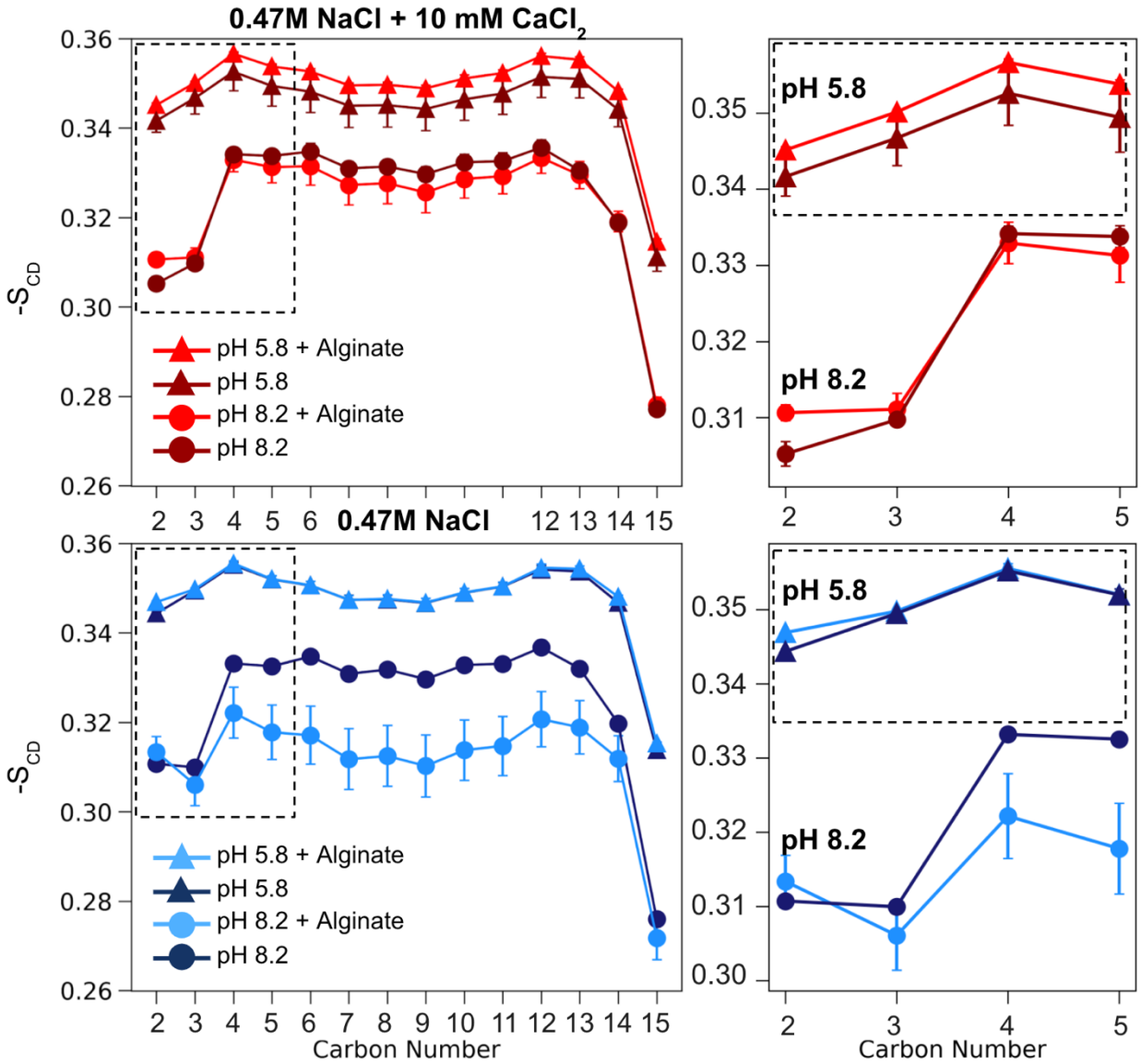

Fig. S16. Local order parameters for all systems, not separated based on protonation state, with close-ups of the carbon C2-C4 regions.

i. IRRAS spectra of alginate co-adsorption via magnesium bridging

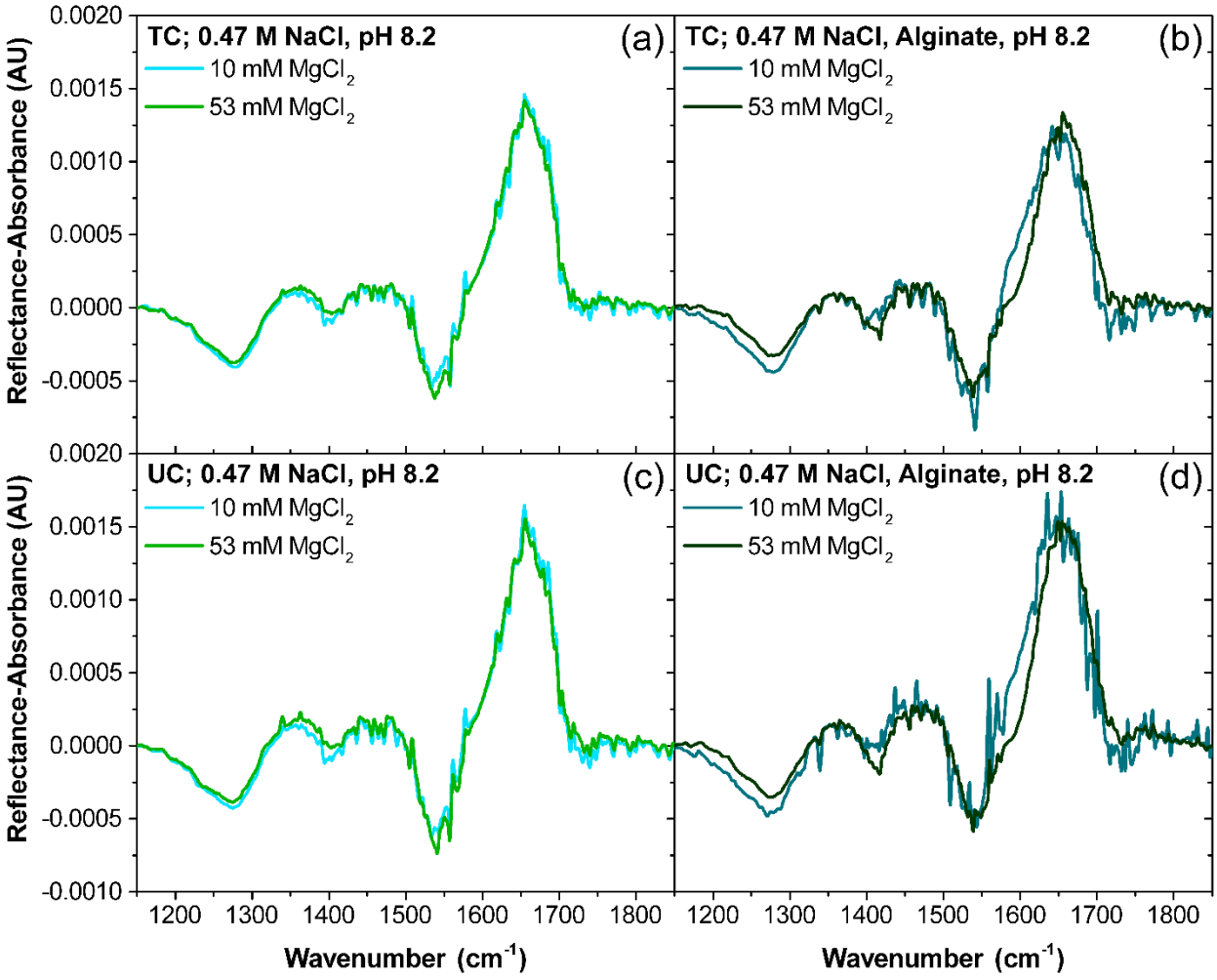

Fig. S17. IRRAS spectra of the COOH stretching region indicate weak alginate co-adsorption to the d_{31}-palmitic acid monolayer via Mg^{2+} bridging interactions. Spectral lines are color-coded to indicate differences in solution composition. Surface pressure was held constant in the (a), (b) tilted condensed (5 mN/m) and (c), (d) untilted condensed (25 mN/m) phases throughout spectral acquisition. Spectra corresponding to the salt water solutions are shown in (a) and (c), and spectra corresponding to the salt water solutions containing 50 ppm alginate are shown in (b) and (d).

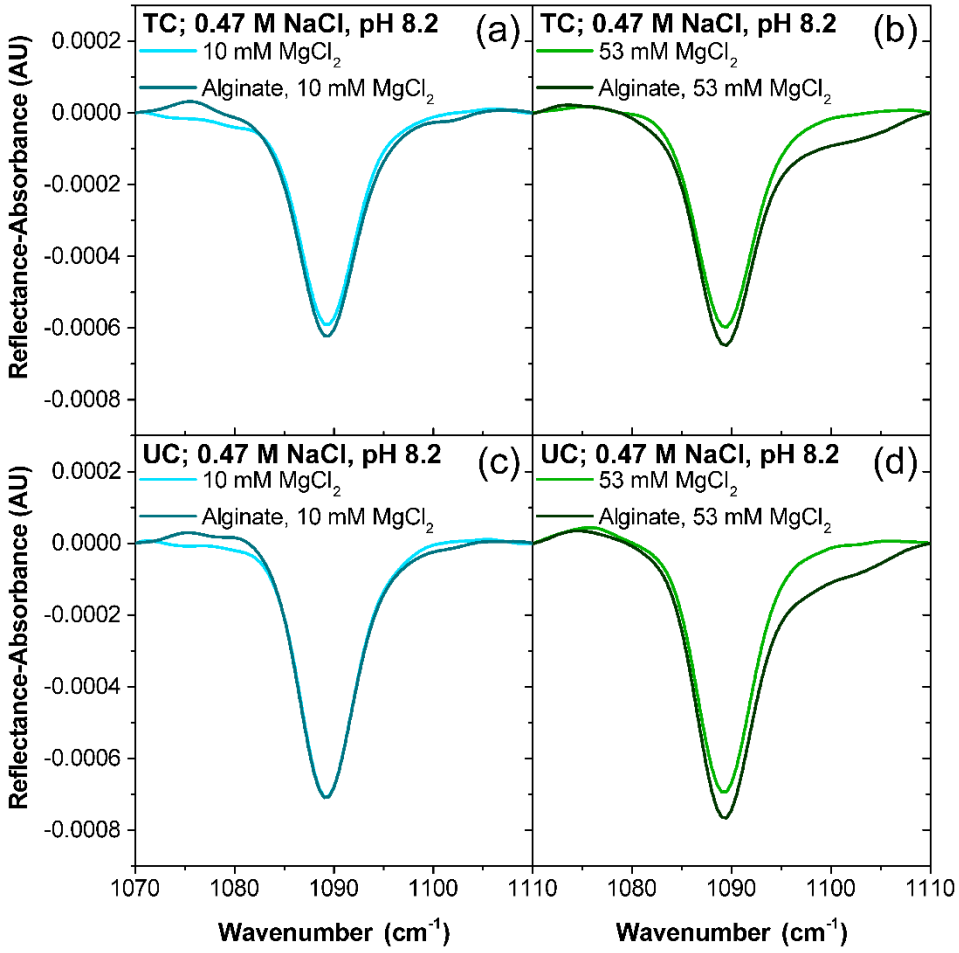

Fig. S18. IRRAS spectra of the CD_2 scissoring mode region demonstrate weak alginate co-adsorption to the d_{31}-palmitic acid monolayer in the presence of 53 mM $MgCl_2$ at pH 8.2, and the spectra indicate no changes in the d_{31}-palmitic acid lattice packing upon adsorption. Spectral lines are color-coded to indicate differences in solution composition. Surface pressure was held constant in the (a), (b) tilted condensed (5 mN/m) and (c), (d) untilted condensed (25 mN/m) phases throughout spectral acquisition.

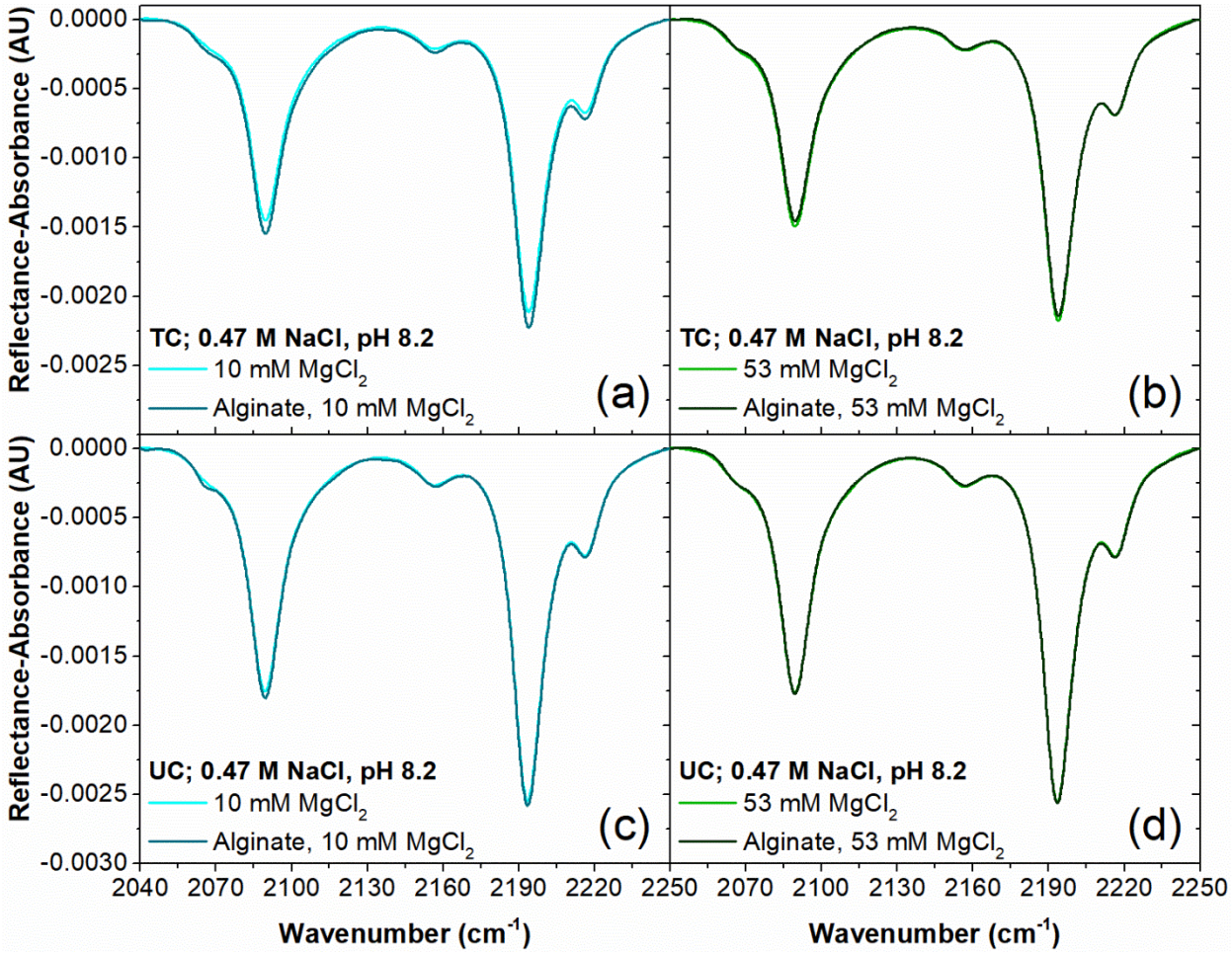

Fig. S19. IRRAS spectra of the C-D stretching mode region demonstrate no changes in the d_{31}-palmitic acid lipid tail packing with alginate co-adsorption, indicating no alginate intercalation into the monolayer. Spectral lines are color-coded to indicate differences in solution composition. Surface pressure was held constant in the (a), (b) tilted condensed (5 mN/m) and (c), (d) untilted condensed (25 mN/m) phases throughout spectral acquisition.

References

1 R. L. Davidchack, R. Handel and M. V. Tretyakov, *J. Chem. Phys.*, 2009, **130**, 234101.
2 T. Darden, D. York and L. Pedersen, *J. Chem. Phys.*, 1993, **98**, 10089–10092.
3 J. Yoo and A. Aksimentiev, *Physical Chemistry Chemical Physics*, 2018, **20**, 8432–8449.
4 K. Han, R. M. Venable, A.-M. Bryant, C. J. Legacy, R. Shen, H. Li, B. Roux, A. Gericke and R. W. Pastor, *J. Phys. Chem. B*, 2018, **122**, 1484–1494.
5 E. Duboué-Dijon, M. Javanainen, P. Delcroix, P. Jungwirth and H. Martinez-Seara, *J. Chem. Phys.*, 2020, **153**, 050901.
6 D. M. de Oliveira, S. R. Zukowski, V. Palivec, J. Hénin, H. Martinez-Seara, D. Ben-Amotz, P. Jungwirth and E. Duboué-Dijon, *Phys. Chem. Chem. Phys.*, 2020, **22**, 24014–24027.

7 M. L. Valentine, A. E. Cardenas, R. Elber and C. R. Baiz, *Biophysical Journal*, 2020, **118**, 2694–2702.
8 C. Lee, A. C. Dommer, J. M. Schiffer, R. E. Amaro, V. H. Grassian and K. A. Prather, *J. Phys. Chem. Lett.*, 2021, **12**, 5023–5029.
9 Y. Shao, Z. Gan, E. Epifanovsky, A. T. B. Gilbert, M. Wormit, J. Kussmann, A. W. Lange, A. Behn, J. Deng, X. Feng, D. Ghosh, M. Goldey, P. R. Horn, L. D. Jacobson, I. Kaliman, R. Z. Khaliullin, T. Kuś, A. Landau, J. Liu, E. I. Proynov, Y. M. Rhee, R. M. Richard, M. A. Rohrdanz, R. P. Steele, E. J. Sundstrom, H. L. W. III, P. M. Zimmerman, D. Zuev, B. Albrecht, E. Alguire, B. Austin, G. J. O. Beran, Y. A. Bernard, E. Berquist, K. Brandhorst, K. B. Bravaya, S. T. Brown, D. Casanova, C.-M. Chang, Y. Chen, S. H. Chien, K. D. Closser, D. L. Crittenden, M. Diedenhofen, R. A. D. Jr, H. Do, A. D. Dutoi, R. G. Edgar, S. Fatehi, L. Fusti-Molnar, A. Ghysels, A. Golubeva-Zadorozhnaya, J. Gomes, M. W. D. Hanson-Heine, P. H. P. Harbach, A. W. Hauser, E. G. Hohenstein, Z. C. Holden, T.-C. Jagau, H. Ji, B. Kaduk, K. Khistyaev, J. Kim, J. Kim, R. A. King, P. Klunzinger, D. Kosenkov, T. Kowalczyk, C. M. Krauter, K. U. Lao, A. D. Laurent, K. V. Lawler, S. V. Levchenko, C. Y. Lin, F. Liu, E. Livshits, R. C. Lochan, A. Luenser, P. Manohar, S. F. Manzer, S.-P. Mao, N. Mardirossian, A. V. Marenich, S. A. Maurer, N. J. Mayhall, E. Neuscamman, C. M. Oana, R. Olivares-Amaya, D. P. O'Neill, J. A. Parkhill, T. M. Perrine, R. Peverati, A. Prociuk, D. R. Rehn, E. Rosta, N. J. Russ, S. M. Sharada, S. Sharma, D. W. Small, A. Sodt, T. Stein, D. Stück, Y.-C. Su, A. J. W. Thom, T. Tsuchimochi, V. Vanovschi, L. Vogt, O. Vydrov, T. Wang, M. A. Watson, J. Wenzel, A. White, C. F. Williams, J. Yang, S. Yeganeh, S. R. Yost, Z.-Q. You, I. Y. Zhang, X. Zhang, Y. Zhao, B. R. Brooks, G. K. L. Chan, D. M. Chipman, C. J. Cramer, W. A. G. III, M. S. Gordon, W. J. Hehre, A. Klamt, H. F. S. III, M. W. Schmidt, C. D. Sherrill, D. G. Truhlar, A. Warshel, X. Xu, A. Aspuru-Guzik, R. Baer, A. T. Bell, N. A. Besley, J.-D. Chai, A. Dreuw, B. D. Dunietz, T. R. Furlani, S. R. Gwaltney, C.-P. Hsu, Y. Jung, J. Kong, D. S. Lambrecht, W. Liang, C. Ochsenfeld, V. A. Rassolov, L. V. Slipchenko, J. E. Subotnik, T. V. Voorhis, J. M. Herbert, A. I. Krylov, P. M. W. Gill and M. Head-Gordon, *Mol. Phys.*, 2015, **113**, 184–215.
10 A. Haug, S. Myklestad, B. Larsen, O. Smidsrød, G. Eriksson, R. Blinc, S. Paušak, L. Ehrenberg and J. Dumanović, *Acta Chem. Scand.*, 1967, **21**, 768–778.
11 E. R. Morris, D. A. Rees, D. Thom and J. Boyd, *Carbohyd. Res.*, 1978, **66**, 145–154.
12 K. Y. Lee and D. J. Mooney, *Prog. Polym. Sci.*, 2012, **37**, 106–126.
13 J. R. Rumble, Ed., *CRC Handbook of Chemistry and Physics*.
14 C. Y. Lin, M. W. George and P. M. W. Gill, *Aust. J. Chem.*, 2004, **57**, 365.